Mg isotope composition of runoff is buffered by the regolith exchangeable pool

Di Cai[1], Michael J. Henehan[1], David Uhlig[2], Friedhelm von Blanckenburg[1]

[1] GFZ German Research Centre for Geosciences; Section 3.3 Earth Surface Geochemistry; Telegrafenberg, 14473 Potsdam, Germany

[2] Forschungszentrum Jülich GmbH, Institute of Bio- and Geosciences (IBG-3), Agrosphere, Wilhelm-Johnen-Str, 52425 Jülich, Germany

Correspondence to: dcai@gfz-potsdam.de

Abstract

In a small, forested catchment underlain by gneiss (Conventwald, Black Forest, Germany), we found that the magnesium isotope composition (δ^{26}Mg) of creek water did not show seasonal variability, despite variations in dissolved Mg concentrations. To investigate the potential controlling factors on water δ^{26}Mg values, we studied the Mg isotope composition of solid samples (bedrock, bulk soil, clay-sized fraction of soil, separated minerals, the exchangeable fraction of regolith) and water samples comprising time series of creek water, groundwater and subsurface flow. Subsurface flow from 0-15 cm depth (-0.80 ± 0.08 ‰) and 15-150 cm depth (-0.66 ± 0.17 ‰), groundwater (-0.55 ± 0.03 ‰), and creek water (-0.54 ± 0.04 ‰) are all depleted in heavy Mg isotopes compared to bedrock (-0.21 ± 0.05 ‰). Subsurface flow samples have similar δ^{26}Mg values to the regolith exchangeable fraction at the respective sampling depths. Also, groundwater and creek water show δ^{26}Mg values that are identical to those of the exchangeable fraction in the deep regolith. We suggest, therefore, that cation-exchange processes in the regolith control Mg concentrations and δ^{26}Mg values of creek water at our study site. This assumption was further verified by batch adsorption-desorption experiments using soil samples from this study, which showed negligible Mg isotope fractionation during adsorption-desorption. We propose that the exchangeable fraction of the regolith buffers dissolved Mg concentrations by adsorbing and storing Mg when soil solutions are high in concentration in the dry season and desorbing Mg when rainfall infiltrates and percolates through the regolith in the wet season. This mechanism may explain the near chemostatic behavior of Mg concentrations and the invariance of δ^{26}Mg values in creek water.

In addition, the depth distribution of exchangeable Mg concentration and isotope composition in the regolith reflects mineral dissolution and secondary mineral formation in deep regolith (> 3 m) and biological cycling in shallower depth (0 – 3m). Magnesium stable isotopes thus provide an accurate snapshot of the geogenic (weathering) and the organic (bio-cycled) nutrient cycle.

1. Introduction

Magnesium (Mg) is a major element in the interior of the Earth and at its surface, the terrestrial hydrosphere, the oceans, and is intensely cycled from the pedosphere into the biosphere. The use of Mg stable isotopes as a tracer to decipher biogeochemical processes in natural systems has evolved in the last two decades into a powerful tool (e.g., Schmitt et al., 2012; Teng, 2017), especially in the Critical Zone - the boundary layer of the Earth that extends from the vegetation canopy down to groundwater.

Laboratory experiments have documented Mg isotope fractionation by both biotic and abiotic processes. Uptake of Mg by plants generally favors heavy Mg isotopes, and Mg translocation within plants can further fractionate Mg isotopes, as demonstrated in growth experiments (Black et al., 2008; Bolou-Bi et al., 2010) and in field studies (e.g., Bolou-Bi et al., 2012; Uhlig et al., 2017). Mycorrhizal fungi associated with the roots might fractionate Mg isotopes too, as evidenced by fungi growth experiments (Fahad et al., 2016; Pokharel et al., 2017). Not all studies observe such fractionations, however, with some studies indicating negligible Mg isotope fractionation during plant uptake (Mavromatis et al., 2014; Kimmig et al., 2018). Abiotic processes are also capable of fractionating Mg isotopes significantly. For example, during the dissolution of olivine, lighter Mg isotopes are preferentially leached at the initial stage of dissolution (Wimpenny et al., 2010; Maher et al., 2016; Pokharel et al., 2019). Granite dissolution experiments show preferential dissolution of isotopically distinct primary minerals (Ryu et al., 2011). During the formation of secondary minerals, some experimental syntheses of brucite (an analogue of octahedrally-coordinated Mg clays), lizardite and kerolite found heavy Mg isotopes to be preferentially incorporated into the octahedral sites (Wimpenny et al., 2014; Ryu et al., 2016). In contrast, elsewhere brucite (Li et al., 2014), and stevensite and saponite (Hindshaw et al., 2020) were found to favor light Mg isotopes. This variable direction of Mg isotope fractionation is thought to be controlled by Mg-O bond length in clay octahedral sites, although a kinetic effect cannot be ruled out (Li et al., 2014; Hindshaw et al., 2020). Compared to the aforementioned processes, less well documented is whether Mg isotopes fractionate during adsorption-desorption processes. In an adsorption experiment (Wimpenny et al., 2014), Mg retained by clays had almost identical or by only ~0.1‰ more

64 negative δ^{26}Mg values than the original Mg solution, suggesting the adsorption of Mg onto clays is
65 associated with little or no Mg isotope fractionation. Similarly, after synthesis of stevensite and
66 saponite, Hindshaw et al., (2020) observed the exchangeable Mg of the synthesized mineral to have
67 a δ^{26}Mg value lower than, or within analytical uncertainty of, the initial solution.
68
69 As with these lab experiments under controlled conditions, the Mg isotope composition of river
70 water show similar complexity. For example, river water has been found to be isotopically lighter
71 than the silicate bedrock it drains due to secondary mineral formation favoring heavy Mg isotopes
72 (Tipper et al., 2006a, b, 2008; Brenot et al., 2008; Ma et al., 2015; Dessert et al., 2015). Conversely,
73 however, in other catchments secondary mineral formation incorporating isotopically light Mg is
74 inferred (Pogge von Strandmann et al., 2008). Since aforementioned lab experiments have
75 identified both fractionation directions during secondary mineral formation (e.g., Wimpenny et al.,
76 2014; Li et al., 2014; Hindshaw et al., 2020), these hypotheses are not incompatible. There have
77 also been cases where isotopic fractionation in rivers could not be attributed to the formation of
78 secondary minerals. For example, in Greenland, river water was found to be too dilute to form
79 secondary minerals. Instead, the negative δ^{26}Mg values in river water were explained by the
80 preferential dissolution of isotopically light calcite (Wimpenny et al., 2011). Elsewhere, in the
81 Southern Sierra Nevada Critical Zone Observatory (SSCZO) creek water was enriched in light Mg
82 isotopes despite the fact that Mg isotope composition of soil was similar to that of bedrock, which
83 was attributed to the preferential uptake of heavy Mg isotopes by plants (Uhlig et al., 2017).
84
85 Given the complexity of natural watersheds (that vary in lithology, climate and vegetation cover),
86 conclusions drawn from field studies can be more useful if a particular one controlling factor can
87 be singled out. To this end, time series of water samples can be used (e.g., Tipper et al., 2012). Such
88 time series water samples could be collected over discrete storm events (Chapela Lara et al., 2017;
89 Fries et al., 2019) such that short-term hydrological change is the main factor driving variation.
90 Alternatively, they can be collected in different seasons (Bolou-Bi et al., 2012; Tipper et al., 2012;
91 Mavromatis et al., 2014; Uhlig et al., 2017; Hindshaw et al., 2019; Novak et al., 2021) to investigate
92 biological and longer-term hydrological effects. However, the response of δ^{26}Mg values to
93 discharge varies among studies. In the studies of Fries et al. (2019) and Hindshaw et al. (2019), Mg
94 concentration and isotope composition changed little compared to discharge variation, while in
95 other studies (e.g., Bolou-Bi et al., 2012; Mavromatis et al., 2014) a clear correlation was found
96 between discharge and δ^{26}Mg values. At the event-scale or over a hydrological season, variations
97 in the Mg isotope composition of river water were either attributed to in-stream mixing of Mg from

different depths or the combined effect of more than one process (Tipper et al., 2012; Mavromatis et al., 2014; Chapela Lara et al., 2017).

To fill gaps in the understanding of Mg isotope fractionation during weathering processes, we conducted a comprehensive study in a small, forested catchment underlain by felsic metamorphic rock (Conventwald, Black Forest, Germany). Along with measurements of the Mg isotope composition of bedrock, bulk regolith, clay-sized fraction, and exchangeable fraction of regolith, we investigated the potential controlling factors on the Mg isotope composition of water. We collected time series samples of not only stream water but also groundwater and subsurface flow from 0-15 cm and 15-150 cm below the surface. We suggest that the vertical distribution of the Mg isotope composition of the exchangeable fraction is due to weathering imprinted by biological cycling. Exchange reactions in our catchment are a primary control on water chemistry as δ^{26}Mg values of water are like those of the exchangeable fraction at depths where it was collected. To further interrogate this finding, adsorption and desorption batch experiments using soil samples from our study site were carried out, indicating negligible fractionation during exchange processes. This combination of field research and lab experiments informs about processes fractionating Mg in the critical zone and further verifies the potential of Mg isotopes as a tool in tracing continental weathering process.

2. Geological setting

Samples were collected from an instrumented forest "Conventwald" (48°02′0N, 7°96′0E), located in the Black Forest, southern Germany. This study site is part of the long-term forest ecosystem monitoring program "International Co-operative Program on assessment and monitoring of air pollution effects on forests (ICP Forest Level II)" and represents also one of the study sites of the DFG priority program SPP 1685 "Ecosystem Nutrition—Forest Strategies for limited Phosphorus Resources". The monitored creek catchment has an area of 0.077 km² and the average elevation was ~840 m.a.s.l.. Mean annual temperature of the study site was 6.8 ˚C, and mean annual precipitation was 1395 mm/yr. The underlying bedrock is paragneiss, which was developed from metamorphosed sedimentary rock in the Precambrian. Weathered bedrock was found at ~7 m depth and unweathered bedrock was encountered at ~16 m depth during a core-drilling campaign. The main Mg-hosting minerals in the bedrock include hornblende, chlorite, biotite. Based on microscopic investigations, chlorite and biotite were formed from metamorphosed hornblende. The

129 soil type is a hyperdystric skeletic folic Cambisol with a loamy or sandy loamy texture and a mor-
130 type moder forest floor atop. A detailed description is provided by Lang et al. (2017). The study
131 site was not glaciated during the Quaternary. Periglacial slope deposits developed during the last
132 glacial maximum. The uppermost meter of soil had a rock fragment content of ~70%. The
133 vegetation is mainly composed of European beech *(Fagus sylvatica*, ~40%) and Norway spruce
134 (*Picea abies*, ~45%). Previous element budget calculations for this site were presented by Uhlig

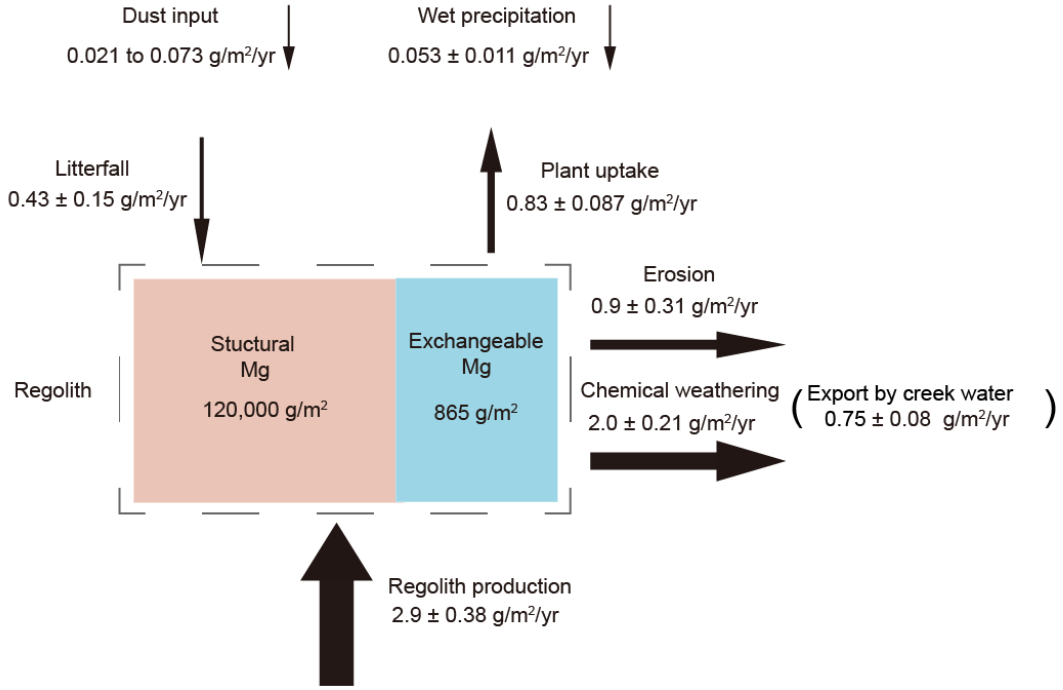

135 and von Blanckenburg, (2019). The result for Mg is shown in Fig. 1 for reference.
136
137 **Fig. 1** Input-output Mg budget of this catchment. Data from Uhlig and von Blanckenburg (2019)
138 and Uhlig et al. (2020). Arrow width corresponds to the flux magnitude. The chemical weathering
139 Mg flux is calculated from the total denudation rate, the Mg concentration in unweathered bedrock
140 and the Mg loss in regolith (τ_{Zr}^{Mg}, section 4.1). The export by creek water Mg flux is calculated from
141 creek discharge and Mg concentrations in creek water.
142

3. Methods

3.1. Sampling

The sampling strategy was presented in detail by Uhlig and von Blanckenburg (2019) for regolith samples and Sohrt et al. (2019) for water samples. Briefly, shallow regolith was sampled at depth increments of 20 cm in a 3 m deep trench. Deeper regolith beyond 3 m was retrieved using diesel-powered wireline core-drilling to ~20 m. Time series water samples were collected from 01.03.2015 to 25.02.2016. Open rainfall and throughfall were collected biweekly in bulk container coved by a netting mesh. Creek discharge and groundwater were collected daily at midnight by autosampler. The groundwater table level was monitored by a pressure probe installed 8.5 m below the surface. Subsurface flow from subsurface flow collectors (see Bachmain and Weiler 2012) was collected at three depths intervals: 0-15 cm, 15-150 cm, and 150-320 cm. Due to limited availability of water samples from 150-320 cm subsurface flow, we only analyzed the other two shallow subsurface flow samples in this study. All the water samples were acidified and stored at 4 ˚C before analysis. Living wood, beech leaves and spruce needles were collected from representative mature and young trees. Roots are not considered in our study due to the difficulties in root sampling whilst preserving the integrity of trees and the chemical pre-treatment required for isotope analysis.

3.2. Extraction of the exchangeable fraction, separation of the clay-sized fraction and primary minerals

Soil and saprolite samples were first oven-dried and sieved to < 2 mm. Two grams of the selected samples were accurately weighed and added to 15 ml acid-cleaned polypropylene centrifuge tubes pre-filled with 14 ml of a 1M NH_4OAc solution. Samples were agitated, and the resulting suspensions shaken on a hotdog roller at 60 rpm for 3 hours. After reaction, the suspensions were centrifuged at 4200 rpm for 30 min, before the supernatant was pipetted off into a syringe and filtered through a 0.2 μm acetate filter. Solutions were then split into two separate aliquots for major element concentration and Mg isotope analysis. Afterward, the NH_4OAc-extracted soil and saprolite samples were twice rinsed with Milli-Q water. The clay-sized fractions of these samples were then extracted by centrifugation following the USGS method (Poppe et al., 2012). To evaluate the Mg isotope composition of different minerals in bedrock, the main Mg-hosting minerals were separated. Bedrock was first crushed and then sieved to 125 μm - 1 mm. The felsic minerals (mainly quartz, and feldspar in this study) were first removed using a magnet separator. Hornblende,

chlorite, and biotite were hand-picked under a microscope. Chlorite and biotite grains, formed from metamorphosed hornblende, generally contained trace relicts of hornblende.

3.3. Mg isotopes adsorption-desorption experiment using topsoil

To investigate whether Mg isotopes fractionate during adsorption and desorption, we conducted a series of batch experiments using topsoil collected at 5 cm depth from our study site. Prior to the batch experiments, the exchange kinetics of Mg on the soil surface was investigated, to determine the reaction time required to reach equilibrium. Two aliquots of 3 g untreated soil samples were soaked in 30 ml pH-neutral $CaCl_2$ (30 μg/g) and $MgCl_2$ (14 μg/g) solutions, respectively. During reaction, 0.5 ml aliquots of solution were pipetted out after 0.5 h, 1 h, 2 h, 4 h and 40 h for Mg concentration measurements. The results of this preliminary experiment indicate that the exchange reaction was rapid, with near-equilibrium reached within 2 - 4 hours (Fig. 2). In the following experiment, soils were reacted with solution for 3 hours: long enough to reach near equilibrium, but not too long so as to avoid potential dissolution of structural Mg in the soil. In the Mg desorption experiment, circumneutral Milli-Q water (pH 6.2), acidified Milli-Q water (pH 3.2) and $CaCl_2$ solutions of different concentration and pH were reacted with untreated soil to desorb exchangeable Mg. After reaction for 3 hours, the suspensions were centrifuged, before the supernatant was pipetted off into a syringe and filtered from remaining solids for major element concentration and Mg isotope analysis. Procedures for the Mg adsorption experiment were largely identical to those of the Mg desorption experiment, except that $MgCl_2$ solutions were used instead of $CaCl_2$ solutions. Similarly, untreated soil samples were immersed in neutral $MgCl_2$ solutions ([Mg] of 0.6 to 61 μg/g) or acidic $MgCl_2$ solutions ([Mg] of 0.6 to 19 μg/g). A detailed description of experimental procedures can be found in the Supplementary Material and the associated data publication (Cai et al. 2021).

198

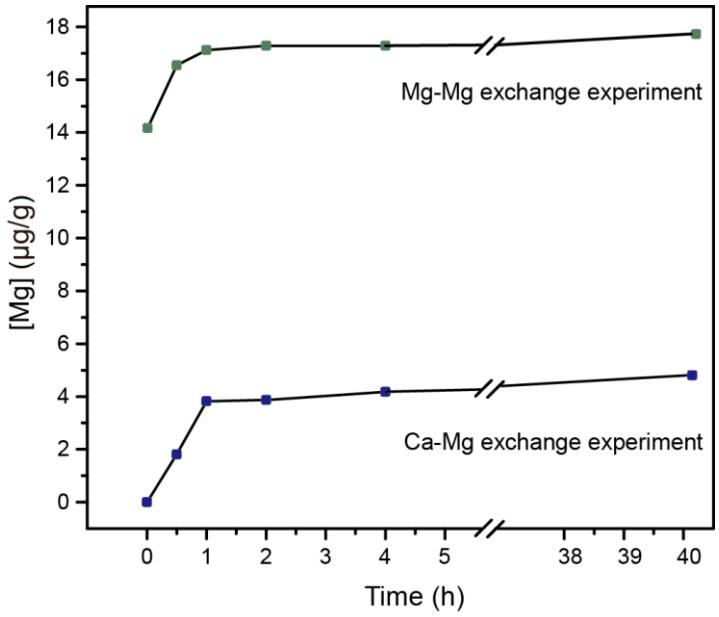

199 **Fig. 2** Kinetics of Mg exchange demonstrated by the magnesium concentration ([Mg]) over time
200 in filtered aliquots of soil suspension solution (see text for details). In both our Ca-Mg and Mg-Mg
201 exchange experiments, near-equilibrium was reached in 2 - 4 hours.

202 ## 3.4. Instrumental methods

203 All measurements were performed in the Helmholtz Laboratory for the Geochemistry of the Earth
204 Surface (HELGES) at GFZ Potsdam. Soil, saprolite, the extracted clay-sized fraction, primary
205 minerals, and bedrock were dissolved by acid digestion using a mixture of concentrated HF and
206 HNO_3 in PFA vials. Aqua regia was also applied to assist digestion after HF and HNO_3 treatment.
207 Elemental concentrations of the filtered supernatant, water samples, and acid digested solution were
208 analyzed by inductively coupled plasma optical emission spectrometry (ICP-OES, Varian 720-ES)
209 following published protocols (Schuessler et al., 2016). Relative uncertainties are better than 5%
210 for Mg based on repeat analyses of the international reference materials SLRS-6 (river water, NRC
211 CNRC), SRM2709a (soil, USGS) and synthetic in-house standards. The chromatography procedure
212 for Mg purification is described in detail in the Supplementary Material and is the same as that used
213 in Uhlig et al. (2017). Magnesium isotopes were measured via multicollector inductively coupled
214 plasma mass spectrometry (MC-ICP-MS, Thermo Scientific Neptune) using DSM3 as bracketing
215 standard to correct for instrumental mass bias (Galy et al., 2003). Analytical results are reported
216 relative to DSM3 in delta notation, $\delta^{x}Mg_{sample} = [({}^{x}Mg/{}^{24}Mg)_{sample} / ({}^{x}Mg/{}^{24}Mg)_{DSM3} - 1] \times 10^{3}$,
217 where x = 26 or 25. Reference materials Cambridge-1 (pure Mg solution), SLRS-6 (river water),

SRM2709a (soil), SRM1515 (apple leaves) are routinely monitored, yielding values of -2.60 ± 0.07‰ (n=24), -1.24 ± 0.14‰ (n=11), -0.16 ± 0.04‰ (n=8), -1.20 ± 0.04‰ (n=3) respectively, which agree well with previously published values (e.g. Shalev et al., 2018).

4. Results

4.1. δ^{26}Mg values in primary minerals, bulk regolith clay-sized fraction, and the exchangeable fraction

Primary Mg-bearing minerals include hornblende, biotite, and chlorite. Both biotite (-0.08 ± 0.05‰) and chlorite (-0.13 ± 0.09‰) are slightly enriched in heavy Mg isotopes compared to hornblende (-0.21 ± 0.05‰). However, reported δ^{26}Mg values of biotite, chlorite and hornblende fall within the range found in earlier studies (e.g. Tipper et al. 2006b, 2012; Ryu et al. 2011, 2016; Chapela-Lara et al. 2017). Other silicate minerals (mainly feldspar and quartz) containing relatively little Mg (contributing less than 10% of total Mg in bedrock) exhibit significantly more negative δ^{26}Mg values (-0.42 ± 0.07‰). Bulk bedrock shows a similar Mg isotope composition to hornblende, consistent with being the major host phase of Mg.

The δ^{26}Mg values of soil and saprolite show little variation and are on average 0.2‰ more positive than bedrock. τ_{Zr}^{Mg}, calculated as $\frac{[Mg]_{sample}/[Zr]_{sample}}{[Mg]_{bedrock}/[Zr]_{bedrock}} - 1$ (Brimhall and Dietrich, 1987), using Zr as the reference element as justified in Uhlig and von Blanckenburg (2019), suggests ~ 70% loss of Mg in the regolith (Fig. 3).

The δ^{26}Mg values of the clay-sized fraction is ~0.1‰ more positive than bulk regolith from which it was separated (Fig. 4). Meanwhile, the exchangeable fraction of the regolith exhibits systematic variation throughout the profile: a decreasing trend in δ^{26}Mg values with depth is observed from 0-1.5 m depth, followed by an increasing trend to -0.52‰ to ~3 m, and below 3 m depth values are largely invariant (Fig. 4). The cation exchange capacity (CEC) of bulk regolith ranges from 0.6 to 8.3 meq/100g (Table S-4). The Mg concentration of the exchangeable fraction relative to the Mg concentration of bulk soil amounts to <0.1% and is thus a negligible contribution to the δ^{26}Mg values of bulk soil.

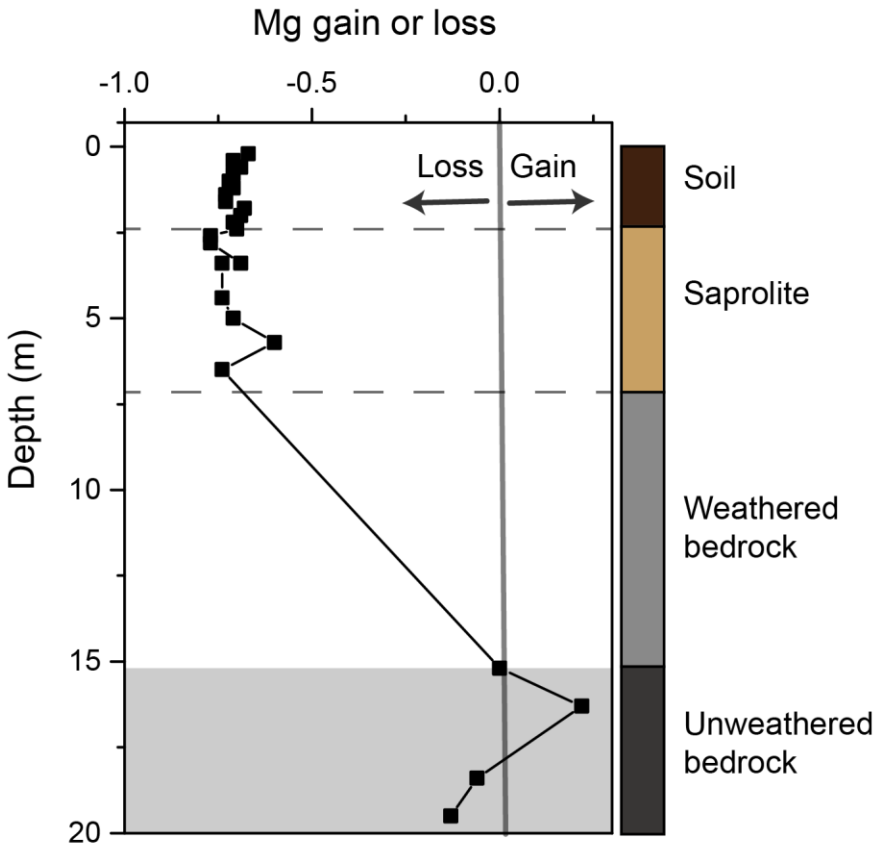

244

245 **Fig. 3** Depth distribution of Mg gain (positive τ_{Zr}^{Mg} values) or loss (negative τ_{Zr}^{Mg} values) in
246 regolith.

247

248 4.2. δ^{26}Mg values of plant samples

249 Plant samples show variable δ^{26}Mg values among species and tissue types (Fig. 4). Beech tree ring
250 samples span a wide range of δ^{26}Mg values from -0.61‰ to -0.39‰ with an average of -0.49 ±
251 0.16‰ (mean ± 2SD, n=5). Twigs and leaves are generally more enriched in heavy Mg isotopes
252 than the trunk. Based on Mg allocation in beech tree tissues (4%, 10%, 69% and 17% for foliage,
253 branch, trunk, and roots, respectively, Feger, 1997), the estimated δ^{26}Mg value of bulk aboveground
254 beech tree is -0.41 ±0.12‰. Roots were not sampled in this study. To estimate their composition,
255 an apparent Mg isotope fractionation factor for translocation of Mg from tree roots to trunk
256 ($\Delta^{26}Mg_{root\text{-}trunk}$) was compiled from previous field studies for sugar maple (Kimmig et al. 2018) and
257 Norway spruce (Bolou-Bi et al. 2012, Novak et al. 2020a,b) and amounts to 0.31 ± 0.38 ‰ (mean
258 ± 2SD, n=6). The estimated δ^{26}Mg value of root is thus ~ -0.11 ‰, and bulk whole beech is ~-
259 0.42 ‰, a value indistinguishable from bulk aboveground beech. Spruce needles (-0.74‰ to -

260 0.87‰) are slightly depleted in ^{26}Mg compared to the trunk and exchangeable Mg. This value is
261 similar to the data reported for needles in a Vosges Mountains Forest (Bolou-Bi et al., 2012) and is
262 amongst the most negative $\delta^{26}Mg$ value compiled for biological samples by Pokharel et al. (2018).

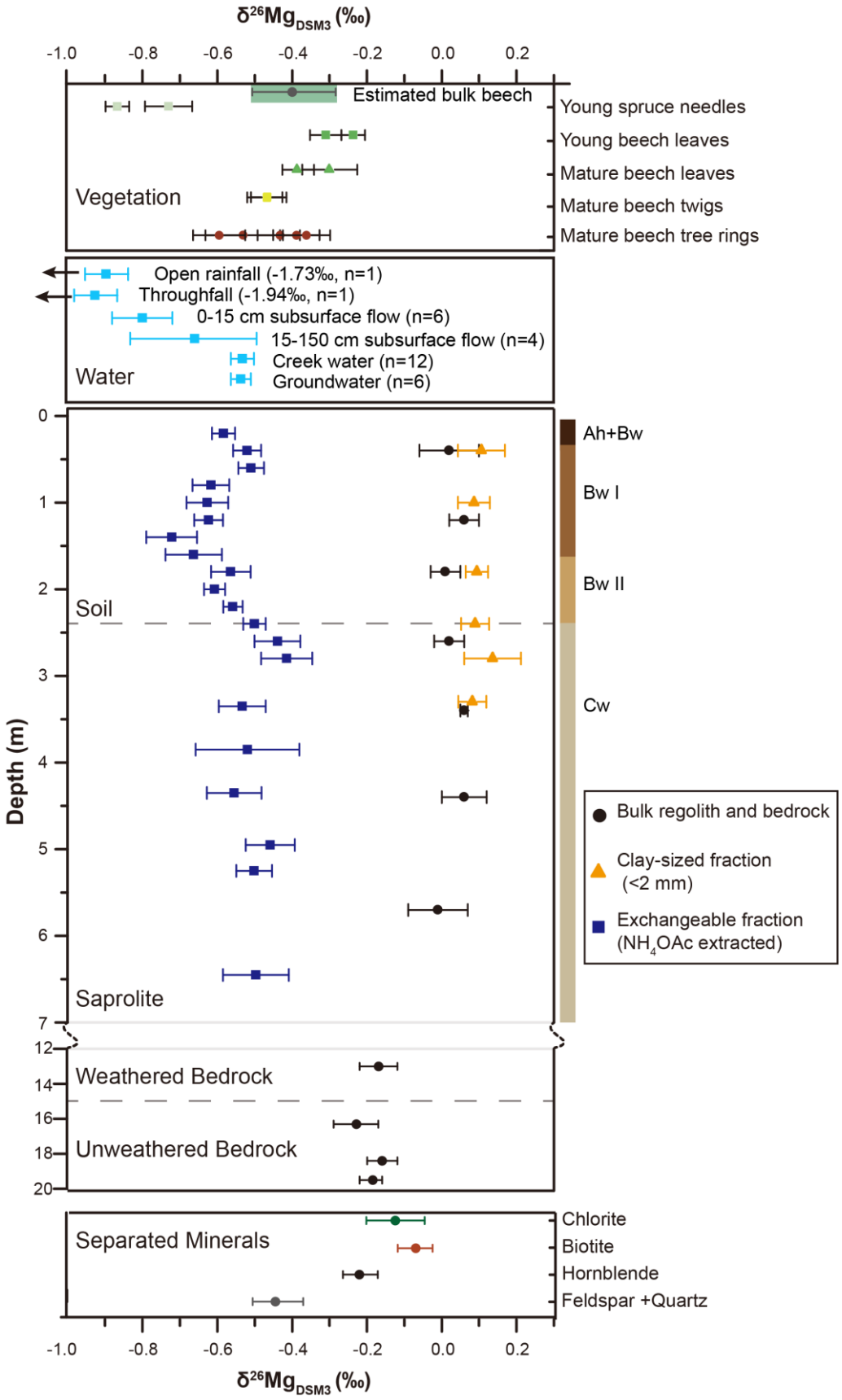
δ26MgDSM3 (‰)
-1.0
-0.8
-0.6
-0.4
-0.2
0.0
0.2
Estimated bulk beech
Young spruce needles
Young beech leaves
Mature beech leaves
Mature beech twigs
Mature beech tree rings
Vegetation
Open rainfall (-1.73‰, n=1)
Throughfall (-1.94‰, n=1)
0-15 cm subsurface flow (n=6)
15-150 cm subsurface flow (n=4)
Creek water (n=12)
Groundwater (n=6)
Water
Depth (m)
0
1
2
3
4
5
6
7
12
14
16
18
20
Soil
Saprolite
Weathered Bedrock
Unweathered Bedrock
Ah+Bw
Bw I
Bw II
Cw
Bulk regolith and bedrock
Clay-sized fraction (<2 mm)
Exchangeable fraction (NH4OAc extracted)
Separated Minerals
Chlorite
Biotite
Hornblende
Feldspar +Quartz
-1.0
-0.8
-0.6
-0.4
-0.2
0.0
0.2
δ26MgDSM3 (‰)

263

Fig. 4 Magnesium isotope composition ($\delta^{26}Mg_{DSM3}$) of bulk regolith, separated minerals, clay-sized fraction, exchangeable fraction, water samples and plant samples. Ah, Bw, Cw: Soil horizons according to IUSS/ISRIC/FAO 2006. For water samples, error bars represent 2SD of the mean value of time series samples. For other samples, error bars represent 2SD of four replicate measurements (similarly hereinafter).

4.3. Mg concentration and δ^{26}Mg values of time series water samples

Subsurface water flow collected from 0-15 cm depth show the largest variation in Mg concentration ([Mg]) among all water samples, ranging from 17 to 184 μmol/l, which is expected due to dilution with open rainfall or condensation through evaporation. δ^{26}Mg values, however, show little variation (-0.80 ± 0.08‰ mean ± 2SD, n=6) across different seasons and hydrological conditions. Despite the shallow depth at which the subsurface flow was collected, these δ^{26}Mg values are significantly more positive than the open rainfall (-1.73 ± 0.03‰) and throughfall (-1.97 ± 0.03‰). Similarly negative δ^{26}Mg values of open rainfall were also observed in the Damma glacier catchment in Switzerland (-1.29 to -1.59 ‰, Tipper et al., 2012) and the Hermine Experimental Watershed in Canada (-1.58 to -2.22 ‰, Kimmig et al., 2018). The negative δ^{26}Mg values of open rainfall may result from the dissolution of carbonate dust in rain (Tipper et al., 2012; Kimmig et al., 2018). The lighter Mg isotopes in throughfall may reflect the leaching of isotopically light Mg from the canopy such as the unbonded Mg contained in cells that is depleted in ^{26}Mg as compared to Mg in Chlorophyll or other bonded Mg forms (Kimmig et al., 2018; Pokharel et al., 2018). Subsurface flow collected from 15-150 cm depth shows relatively smaller [Mg] variation, ranging from 19 to 49 μmol/l and on average, Mg concentrations are lower than for the 0-15 cm depth section. Except for one subsurface flow sample from 15-150 cm depth collected in August, which has identical δ^{26}Mg values (-0.84 ± 0.03‰) to that collected from the 0-15 cm depth section, subsurface flow samples collected from 15-150 cm depth show consistently more positive δ^{26}Mg values than their shallower counterparts (-0.62 ± 0.04‰, n=3).

Groundwater [Mg] is generally twice as high in concentration as 15-150 cm subsurface flow, and ranges between 65 and 99 μmol/l. Despite changing [Mg], δ^{26}Mg values of groundwater remain invariant (-0.55 ± 0.03‰, n=6). However, although discharge variations span two orders of magnitude, [Mg] at low flow is only twice as high than [Mg] during high flow periods. Intriguingly, despite the large variability in discharge and the minor variability in [Mg] over the sampling period,

no corresponding change in the $\delta^{26}Mg$ value of creek water was observed (-0.54 ± 0.04‰, n=12), with values remaining identical to that of groundwater.

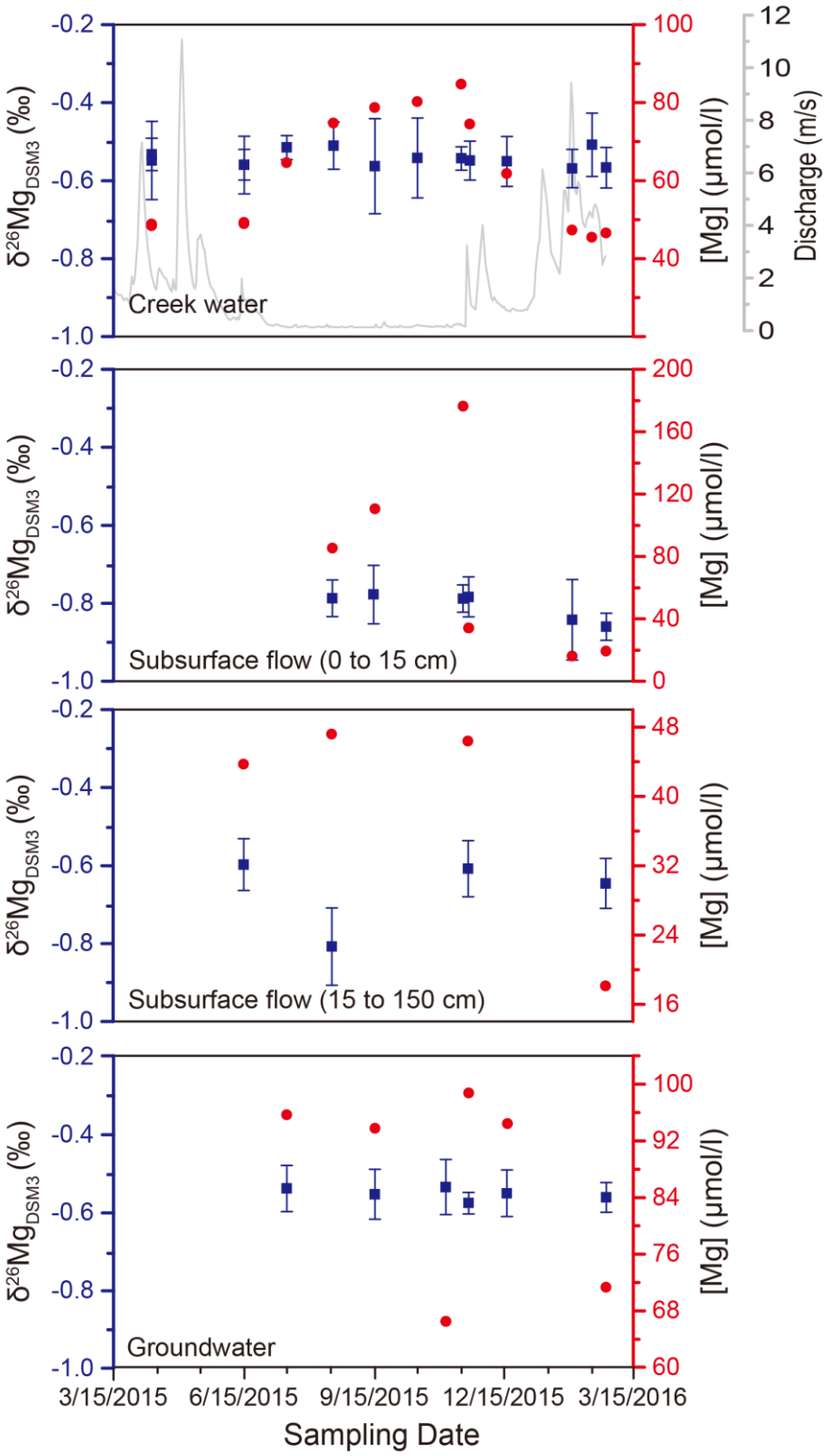

Fig. 5 Magnesium isotope composition ($\delta^{26}Mg_{DSM3}$, left axis) and Mg concentration ([Mg], right axis) of time-series water samples including creek water, subsurface flow and groundwater sampled from a well at 8 m depth. The grey curve in the background of the uppermost panel shows the creek discharge.

4.4. Adsorption and desorption experiment on topsoil

4.4.1. Mg desorption experiment

Assuming excess NH_4OAc could extract all the exchangeable Mg from soil, we found that 20% of Mg was desorbed with circumneutral Milli-Q water (pH 6.2) and 32% was desorbed with Milli-Q acidified to pH 3.2 with a few drops of distilled HNO_3. In both acidic and circumneutral conditions, increasing [Ca] in solution could exchange more Mg, although the increase in Mg desorbed with higher Ca input is considerably weaker at low pH compared to circumneutral pH (Fig. 6a). Importantly, however, despite the difference in the amount of Mg desorbed, the $\delta^{26}Mg$ value of all reacted solutions remain almost identical or slightly more negative (< 0.1‰) than that of bulk soil exchangeable Mg (Fig 6b), suggesting the exchangeable Mg was congruently released to the solutions with little or no fractionation.

4.4.2. Mg adsorption experiment

Patterns of Mg adsorption (and desorption) equilibrium after soil was reacted with $MgCl_2$ solutions are shown in Fig. 6. Data points above the 1:1 line indicate increasing $[Mg]_{solu}$ after reaction, thus a net desorption, while those below the 1:1 line suggest net adsorption during the experiment (Fig. 6c). This result suggests that desorption and adsorption on natural soil depends on both solution pH and input solution Mg concentration. After reaction, regardless of whether adsorption or desorption was dominant, exchangeable Mg had $\delta^{26}Mg$ values that were almost identical to solution Mg (Fig. 6d), suggesting that isotope fractionation is negligible.

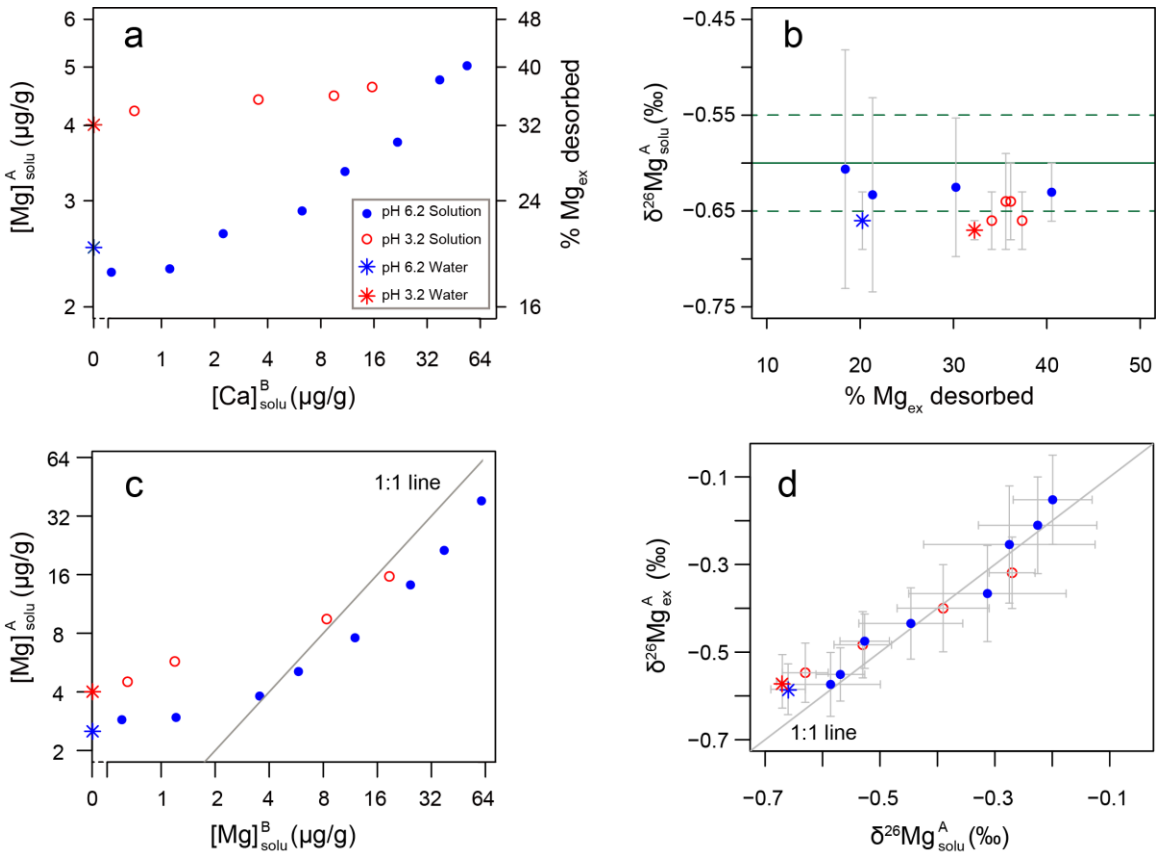

Fig. 6 Results of adsorption-desorption experiments. **Panel a)** depicts the influence of the calcium concentration in the solution ([Ca]) on the amount of desorbed Mg. $[Ca]^{B}_{solu}$ denotes Ca concentration in the solution before reaction. $[Mg]^{A}_{solu}$ denotes the Mg concentration in the solution after reaction. The right-hand y-axis shows the percentage of total exchangeable Mg that is desorbed. Both axes are in log scale. The star symbols denote circumneutral or pH 3.2 water. **Panel b)** shows the relationship between the proportion of Mg desorbed and the isotope composition of desorbed Mg ($\delta^{26}Mg^{A}_{solu}$). Horizontal solid and dashed lines represent the δ^{26}Mg value and its analytical uncertainty (2SD) of the exchangeable fraction of the sample used for the desorption experiment. The data suggests that Mg was released with no or little fractionation. **Panel c)** Mg concentrations in solutions before ($[Mg]^{B}_{solu}$, x-axis) and after ($[Mg]^{A}_{solu}$, y-axis) reaction respectively. Data points above the 1:1 line imply desorption while points below the line imply adsorption. Both axes are in log scale. **Panel d)** Mg isotope composition of solution ($\delta^{26}Mg^{A}_{solu}$) and absorbed fraction ($\delta^{26}Mg^{A}_{ex}$) after reaction. The data points are generally distributed along the 1:1 line, indicating negligible fractionation between solution Mg and exchangeable Mg after reaction.

5. Discussion

5.1. The absence of isotope fractionation during adsorption-desorption experiments

Our lab experiments suggest that soil exchangeable Mg is congruently desorbed to solution without isotope fractionation, regardless of pH, solution chemistry or proportion of Mg released. Similarly, no or very small (<0.1‰) fractionation was observed in Mg adsorption experiments, even though pH exerted a strong influence on the adsorption-desorption equilibrium. We infer that Mg adsorption is non-specific in the sense that it does not involve changes in inner-sphere complexation. The rationale is as follows: if Mg were adsorbed as an inner-sphere complex, then isotopic fractionation might be expected during the process of dehydration and formation of covalent bonds. For example, molecular dynamics simulations of Mg isotope fractionation amongst aqueous Mg species predict fractionations in the range of one to several per mil (Schott et al., 2016). In this case, hydrated Mg, typically represented as $Mg[H_2O]_6^{2+}$ in molecular dynamics simulations (Trivedi and Axe, 2001), is electrostatically attracted to the surface without undergoing dehydration and forming chemical bonds, and thus no isotope fractionation occurs. That Mg is readily exchanged by Ca lends support to this interpretation. In line with Charlet and Sposito (1989), our study showed that Mg adsorption is depressed when solution electrolyte concentration increases, a characteristic of non-specific sorption mechanism.

5.2. Mg isotope fractionation in regolith: preferential dissolution and secondary mineral formation

In the upper ~7 m the $\delta^{26}Mg$ value of bulk regolith (soil and saprolite) is ~ 0.03‰, a value in between that of the remaining primary minerals (biotite and chlorite) and the clay-sized fraction (Fig. 4), and on average 0.2‰ more positive than bedrock. In previous field studies, secondary mineral formation has been widely assumed to be the main factor fractionating Mg isotopes in soil (e.g., Teng et al., 2010; Liu et al., 2014). However, we observed that minerals separated from bedrock are heterogeneous in their Mg isotope composition. Among the main Mg-bearing minerals, biotite and chlorite are more enriched in ^{26}Mg than hornblende. Thus, differential dissolution of primary minerals might cause the observed depletion in ^{24}Mg in regolith. Indeed, X-ray diffraction analyses suggests that hornblende, the Mg phase with a low $\delta^{26}Mg$ value (-0.21‰) is abundant in

the bedrock but undetectable in the upper 7 m of regolith (Uhlig and von Blanckenburg, 2019), suggesting it has been dissolved due to its higher solubility. Therefore, the more positive Mg isotope composition we observed in soil and saprolite might be due to dissolution of hornblende. However, biotite (-0.13‰) and chlorite (-0.08‰), the remaining two Mg carriers, are still by ~0.1‰ isotopically lighter than the bulk soil and saprolite (0.03 ± 0.06‰, n=6). We thus explore next whether secondary mineral formation causes the difference in the Mg isotope composition between bedrock and regolith.

The clay-sized fraction was extracted from regolith and yields a δ^{26}Mg value of 0.10 ± 0.04‰ (n=6), a value more positive than bulk regolith and separated minerals. Because the clay-sized fraction is composed of truly neoformed secondary minerals and fine primary minerals, the δ^{26}Mg values of the secondary minerals are assumed to be even more positive than the mixture. An upper approximation of the relative amount of neoformed secondary minerals can be estimated by a simple mass balance (equation 1).

$$\delta^{26}Mg_{soil} = (1 - f_{secondary}) \times \delta^{26}Mg_{primary} + f_{secondary} \times \delta^{26}Mg_{secondary} \quad (1)$$

In equation 1 $\delta^{26}Mg_{primary}$ represents the mean δ^{26}Mg value of biotite and chlorite (-0.11‰), $\delta^{26}Mg_{secondary}$ is the most positive δ^{26}Mg value of our separated clay-sized fraction (0.12‰), and $f_{secondary}$ is the relative proportion of neoformed secondary minerals. Given that $f_{secondary}$ amounts to ~52%, half of the soil Mg is hosted in secondary minerals. The incorporation of heavy Mg isotopes into clays is also supported by the low δ^{26}Mg value in the remaining fluid (e.g., subsurface flow water) and the exchangeable fraction; a topic we return to section 5.3.2.

In summary, we suggest that the positive δ^{26}Mg value of the regolith is due to a combination of 1) dissolution of isotopically light hornblende and 2) secondary mineral formation further fractionating Mg isotope in regolith towards more positive δ^{26}Mg values.

5.3. Source and vertical distribution of isotopically light exchangeable Mg

The vertical distribution of the Mg concentration and Mg isotope composition of the exchangeable fraction can be divided into two parts: from 0 to 3 m, showing a bulge pattern with low Mg concentrations and more negative δ^{26}Mg values in the center of the bulge; and from below 3 m depth, where Mg concentration and δ^{26}Mg values of the exchangeable fraction are almost invariant

406 (Fig. 7), a pattern similar to that found by Kimmig et al., (2018). Whereas the vertical distribution
407 of element concentrations in the exchangeable fraction has been explained in previous studies
408 through supply from atmospheric deposition, dissolution of primary minerals, and biological
409 cycling (Jobbágy and Jackson, 2001; James et al., 2016; Uhlig and von Blanckenburg, 2019; Yu et
410 al., 2020), the depth distribution of the Mg isotope composition remains poorly constrained.
411

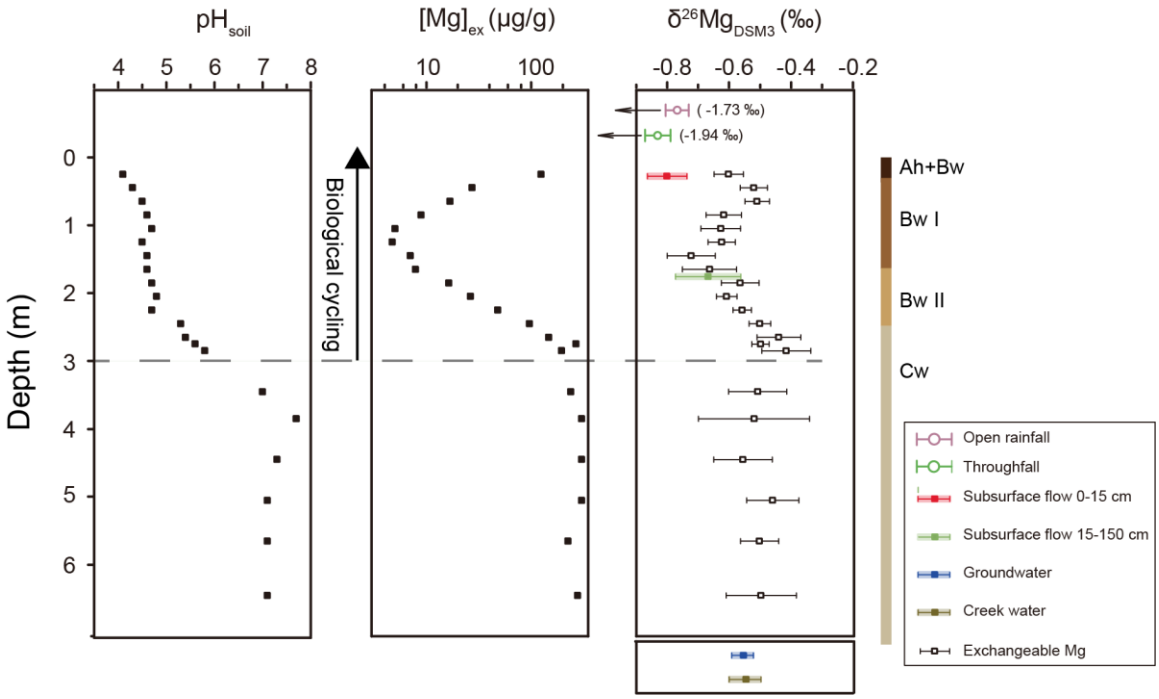

412 Fig. 7 Vertical distribution of soil pH (pH_{soil}), Mg concentration ($[Mg]_{ex}$) and Mg isotope
413 composition ($\delta^{26}Mg_{DSM3}$) of the exchangeable fraction (1M NH_4OAc). The bulged distribution of
414 $[Mg]_{ex}$ and $\delta^{26}Mg$ values in shallow soil (0 – 3 m) is attributed to chemical weathering imprinted
415 by biological cycling, which increases from 3 m depth (dashed line) to the top of the soil profile
416 (indicated by the arrow, see text for detail). The $\delta^{26}Mg$ values of water samples including open
417 rainfall (n=1), throughfall (n=1), subsurface flow from 0-15 cm (n=6) and 15-150 cm depth (n=4),
418 groundwater (n=6), and creek water (n=14) was also shown for comparison.
419

420 **5.3.1. Biological impact on the Mg concentration and isotope composition of the**
421 **exchangeable fraction at shallow regolith (0 to 3 m)**

422 The biological nutrient uplift hypothesis from Jobággy and Jackson (2001) describes how mineral
423 nutrients are biologically uplifted and recycled; in other words, plants take up mineral nutrients
424 from depth and return them to the forest floor via litterfall, from which they can be readily re-
425 utilized. Consequently, concentrations of mineral nutrients in the exchangeable fraction of soil

increase from depth to topsoil. However, previous studies lack direct evidence that elements hosted in the exchangeable fraction of topsoil can be attributed to biological uplift. Our new dataset comprising the paired analyses of Mg concentrations and isotope compositions allows for an assessment of the biological nutrient uplift hypothesis.

The depth profile of the Mg concentration of the exchangeable fraction was described earlier in Uhlig and von Blanckenburg (2019). Importantly, the increasing Mg concentration from 1.5 m depth to topsoil was attributed to biological uplift, which agrees with the studies of Jobbágy and Jackson (2001, 2004). In this case, Mg is utilized by trees at depth (1.5 - 3 m) with heavy Mg isotopes being favored, which agrees with results from $^{87}Sr/^{86}Sr$ and $^{10}Be(meteoric)/^{9}Be$ ratios used as nutrient uptake tracer in Uhlig et al. (2020). The Mg is then cycled through trees and a fraction is ultimately returned to the forest floor via annual litterfall. As Mg is not significantly re-utilized from organic matter in this study site (Uhlig and von Blanckenburg 2019), isotopically heavy Mg liberated from decomposing plant litter or organic matter may re-enter the pool of the exchangeable fraction.

In support of this suggested mechanism the increase of both $[Mg]_{ex}$ and $\delta^{26}Mg_{ex}$ values from 1.5 m to the forest floor is consistent with the observation that beech leaves (representing plant litter) are enriched in heavy Mg isotopes. Even though Uhlig and von Blanckenburg (2019) concluded that trees do not set the stoichiometry of the exchangeable fraction of the upper three meters of soil, their general statement may not hold for elements such as Mg that are not significantly re-utilized. In summary, we conclude that the $\delta^{26}Mg_{ex}$ value of the top 3 m of our profile is first set by secondary mineral formation (see below), to be then overprinted by Mg uptake by trees (at 1.5 to 3 m depth) and biological uplift of Mg (in the top 1.5 m).

5.3.2. Source of isotopically light Mg in the exchangeable fraction of deep regolith (>3 m)

The exchangeable fraction of deep regolith (>3 m) is characterized by high Mg concentrations and low $\delta^{26}Mg$ values. Previous studies (e.g., Opfergelt et al., 2014; Chapela Lara et al., 2017; Uhlig et al., 2017; Kimmig et al., 2018) also found that the exchangeable fraction is generally isotopically lighter than bulk regolith. Opfergelt et al. (2014) attributed this phenomenon to isotope fractionation during successive adsorption-desorption processes. However, our adsorption-desorption experiment using topsoil from our study site shows negligible isotope fractionation. Therefore, other factors need to be considered. Both open rainfall and throughfall are depleted in isotopically heavy Mg, but this isotope signature is not likely transferred to several meters depth as demonstrated by a labeling experiment with an artificial ^{26}Mg spike (van der Heijden et al., 2013). In addition, the inventory of the exchangeable Mg pool is more than 10^3 times higher than the

annual influx of Mg by atmospheric deposition (Fig. 1). Because the chemical weathering flux of Mg exceeds Mg input by open rainfall by about 40 times, the large exchangeable Mg pool is thought to originate from weathering of the regolith rather than from atmospheric input. Felsic minerals (feldspar and quartz) exhibit δ^{26}Mg values similar to exchangeable Mg (Fig. 4), but the Mg concentration in these minerals is too low to be a primary Mg source, amounting to less than 10% relative to biotite and chlorite. Moreover, biotite is more soluble than the felsic minerals (e.g., 1.5×10^{-10} mol/g/s for biotite compared to 6.6×10^{-11} mol/g/s for plagioclase in a granite dissolution experiment, Ganor et al., 2004). The isotopically light Mg of the exchangeable fraction thus does not originate from the dissolution of felsic minerals. Carbonate minerals are known to have the most negative δ^{26}Mg values in environmental samples (Saenger and Wang, 2014), but microscopic and XRD (Uhlig and von Blanckenburg 2019) analyses failed to identify the presence of carbonate minerals at this site. Eliminating these factors, the most likely process driving the Mg isotope composition of the exchangeable fraction to negative δ^{26}Mg values is secondary mineral formation as discussed in section 5.2. It is likely that the Mg residue in soil water entered the exchangeable pool after secondary mineral formation. This is evidenced by former clay synthesis experiments (Hindshaw et al., 2020), which showed 17 - 33 % Mg hosted in exchangeable sites compared to Mg in bulk solid.

To identify the surfaces providing exchangeable sites in deep (>3 m) regolith (such as organic matter, phyllosilicates, oxides and hydroxides), we combined mineralogical evidence (XRD analyses in Uhlig and von Blanckenburg (2019)) with the cation exchange capacity (CEC, Table S4). CEC of deep regolith ranges from 5.7 to 8.3 meq/100g. Since most primary minerals like quartz and feldspar have negligible exchange capacity, the CEC of minerals providing exchange sites in the deep regolith will exceed 8.3 meq/100g. As humus with a high CEC of >150 meq/100g (Brady and Weil 2008) can be ruled as major exchangeable site host in the deep regolith, and oxides have a low CEC of <10 meq/100g (Brady and Weil 2008), phyllosilicates likely provide the required exchangeable sites. Identified phyllosilicates in large abundance by XRD (Uhlig and von Blanckenburg 2019) and thin section investigation include chlorite and biotite, which indeed have high CEC (10-40 meq/100g, Brady and Weil 2008). Smectites and vermiculites also have high CEC (80-175 meq/100g, Brady and Weil 2008), but could not be distinguished from biotite using XRD analyses on bulk soil. We thus conclude that the light Mg remaining in solution after formation of secondary minerals is adsorbed onto the exchangeable sites of chlorite and biotite.

5.4. Exchangeable fraction as first order control on runoff water chemistry

It is intriguing that the subsurface flow, groundwater, and creek water show negligible seasonal variation in $\delta^{26}Mg$ values despite variations in Mg concentration and hydrological condition (Fig. 5). More intriguing, $\delta^{26}Mg$ values of water agree with those of the exchangeable fraction at their respective sampling depth (Fig. 7). For example, groundwater and creek water samples yield almost identical $\delta^{26}Mg$ values to that of the deep regolith (> 3 m) exchangeable pool, and subsurface flow (15 – 150 cm) samples exhibit uniform $\delta^{26}Mg$ values that correspond to the value of exchangeable $\delta^{26}Mg$. As our exchange experiments indicate negligible isotope fractionation during adsorption-desorption (Fig. 6), we hypothesize that the water samples in this study site are in equilibrium with exchangeable pool of corresponding depth. Only in the 0-15 cm subsurface water $\delta^{26}Mg$ values deviate from the exchangeable pool, being on average ~0.2‰ more negative (Fig. 7). A potential explanation for this discrepancy is the contribution of throughfall, in which Mg has a very negative $\delta^{26}Mg$ value. Given the short water flow path length scale of about 15 cm the timescale for desorption may be too low to fully buffer diluted rainwater in terms of concentrations and isotope compositions.

Compared to the invariance of the Mg isotope composition in creek water, Mg concentrations dropped by about half when discharge increased by about two orders of magnitude (Fig 8a). This relationship of concentration (C) and discharge (Q) can be described by the power law equation $C=aQ^b$, with a and b being fitted parameters (Godsey et al., 2009). A log-log slope (b-value) of zero represents chemostasis (Godsey et al., 2009) meaning the concentration of a given solute remains constant regardless of discharge, and a b-value of -1 indicates pure dilution behavior. The b-value of -0.13 in this study (Fig.8a) indicates a strong buffering of the Mg concentration, consistent with observations elsewhere (e.g., Godsey et al., 2009; Clow and Mast, 2010; Kim et al., 2017).

However, the processes causing this buffering effect on cation concentrations are subject to debate (e.g., Maher, 2010; Trostle et al., 2016; Torres et al., 2017; Kim et al., 2017; Torres and Baronas, 2021). What generally missing in previous C-Q studies is direct evidence on the source of Mg supplied to runoff in periods of high water flow. We suggest that it is cation exchange process that buffers Mg concentration in this study site for two reasons. The first reason is the large size of exchangeable Mg in the regolith. Exchangeable Mg hosted in the upper 7 m of regolith lasts for as much as for about 1200 years before being exhausted by solute runoff export into runoff export in this study site (Fig. 1). The second reason is the aforementioned similarity of $\delta^{26}Mg$ values in dissolved phase and corresponding exchangeable fraction (Fig. 7).When rainwater of low cation

concentrations infiltrates into regolith, the water is either initially stored in the vadose zone, or directly recharges groundwater and runoff (e.g. Montgomery and Dietrich 2002; Salve et al., 2012; Sprenger et al, 2016; Kim et al., 2017). This infiltrating water inevitably exchanges cations with the exchangeable pool, which, based on our adsorption-desorption experiments may take place within minutes and reach near-equilibrium in ~ 2 hours (Fig. 2). Soil column leaching experiments have also resulted in significant contributions of exchangeable Mg to the effluent solutions within 60 minutes (Oh and Richter Jr. 2004).

However, the buffering capacity of the exchangeable pool on infiltrating water reaches a limit during prolonged rainfall events at a so-called "set-point" when dilution effects begin to prevail (Godsey et al. 2019). This limitation is also verified by column leaching experiments showing a decreasing trend of base cations desorbed into leachates at prolonged leaching time (Oh and Richter Jr. 2004; Pogge von Strandmann et al., 2020). As a result, slightly dilution (also buffered compared to pure dilution) effect was seen due to the attenuated exchange reaction. Importantly, even if such dilution prevails, the Mg isotope composition remains unaffected as desorption does not fractionate Mg isotopes (Fig. 6b). When it comes to dry season, Mg concentrations are generally higher in soil water and groundwater due to evaporation and mineral dissolution (caused by longer residence times of water, Maher, 2010; Kim et al., 2014). Therefore, Mg tend to be adsorbed to the exchangeable sites in dry seasons to replenish the exchangeable pool. As such, we propose that the exchangeable pool acts like a buffer regulating Mg concentrations and isotope compositions under a range of hydrological conditions. In support of this hypothesis, we note that our batch Mg adsorption experiments (Fig. 6c) have shown the transition from net desorption to net adsorption with increasing solution Mg concentrations. This explanation may also hold for other studies (e.g. Hindshaw et al., 2019; Fries et al., 2019; Novak et al., 2021) that also showed almost invariant δ^{26}Mg values and buffered Mg concentrations in time series runoff samples.

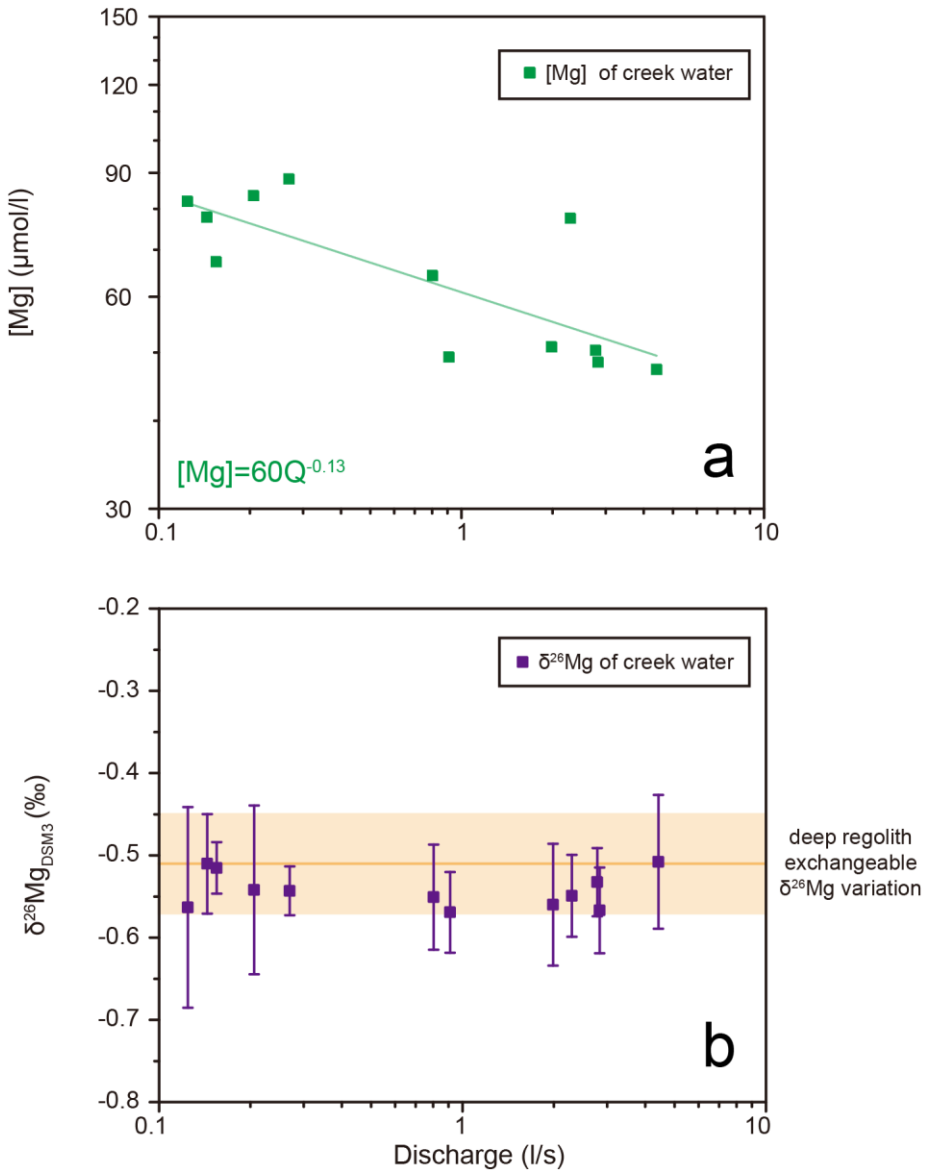

549

550

551 Fig. 8 **a**: Relationship of Mg concentration ([Mg]) with discharge (Q). The Mg concentration is
552 buffered during high flow periods. **b**: Relationship of the Mg isotope composition ($\delta^{26}Mg$) with
553 discharge of creek water. Horizontal line and shaded area illustrate the mean $\delta^{26}Mg$ value ± 2SD of
554 the exchangeable fraction in deep regolith (>3m).

555

5.5. Quantifying dissolved Mg loss by elemental and isotope mass balance

In the critical zone, bulk soil integrates the long-term weathering process and water chemistry is the instantaneous weathering product. Using an isotope mass balance approach, Bouchez et al. (2013) developed an isotope model that quantifies the relationship between the weathering flux of the element of interest and the total denudation flux solely by metal isotopes (equation 2).

$$w^{Mg} = \frac{\delta^{26}Mg_{regolith} - \delta^{26}Mg_{rock}}{\delta^{26}Mg_{regolith} - \delta^{26}Mg_{creek\ water}} \quad (2)$$

In equation 2, w^{Mg} is the fraction of dissolved Mg export relative to the total export of solute and particulate Mg. $\delta^{26}Mg_{regolith}$, $\delta^{26}Mg_{rock}$, and $\delta^{26}Mg_{creek\ water}$ are the δ^{26}Mg values of regolith, bedrock and creek water, respectively. The calculated w^{Mg} is 41 ±11%, indicating that ~41% of total denuded Mg occurs in dissolved form, while the remainder is eroded in particulate form. w^{Mg} can also be evaluated by calculating the relative mass loss of Mg from regolith (τ_{Zr}^{Mg}, Fig. 4). This method gives a value of 71 ± 17%. The results derived from these two methods are roughly consistent, indicating the robustness of using both methods for evaluation of Mg weathering intensity in the critical zone.

6. Conclusion

We hypothesized that the exchangeable fraction exerts the main control on the Mg isotope composition of creek water. Two lines of evidence support this hypothesis: First, results of our laboratory adsorption-desorption experiment show that isotope fractionation during adsorption-desorption processes is negligible and creek water also show δ^{26}Mg values that are identical to those of the exchangeable fraction in the deep regolith. Second, the pool size of exchangeable Mg suffices over millennia to buffer Mg concentrations in creek water. Thus, the exchangeable fraction of Mg records the Mg isotope composition of the fluid. Moreover, we propose that the pool of exchangeable fraction acts like a buffer regulating water Mg concentrations within a range of hydrological conditions: adsorbing and storing cations in dry seasons, when soil solutions are high in cation concentration, and desorbing cations, when rainwater infiltrates into and percolates through the regolith.

We also demonstrate that the vertical distribution of both exchangeable Mg concentration and isotope composition can be reconstructed at high depth resolution in the critical zone. Deep regolith (>3 m) hosts substantial amounts of exchangeable Mg sourced by chemical weathering processes and secondary mineral formation. In contrast, at shallow depth (<3 m) biological cycling significantly overprints the geogenic-impacted Mg isotope composition of the exchangeable fraction through Mg uptake by trees which reaches a depth of up to ~3 m.

Acknowledgements

The authors are grateful for funding from the German National Science Foundation Priority Program 1685 "Ecosystem nutrition: forest strategies for limited phosphorus resources" and to Friederike Lang for coordination and discussion. Di Cai is grateful for funding by a CSC scholarship. Johannes Glodny is acknowledged for support on mineral separation. The authors are grateful to the analytical support provided by Jutta Schlegel and Josefine Holtz. Finally, the authors are grateful to the fruitful reviews by Sara Kimmig, two anonymous reviewers and the associate editor Nathalie Vigier that helped to improve the manuscript.

Data availability statement

The data set including Tables S1–S6 of this study is accessible in the data repository under the reference Cai et al. 2021. https://dataservices.gfz-potsdam.de/panmetaworks/review/e91c6bb09610c102c8b650b0c81971f370c7d8c79851bd61ff81d205720c553e/

References

Anderson S. P., Dietrich W. E., Torres R., Montgomery D. R. and Loague K. (1997) Concentration-discharge relationships in runoff from a steep, unchanneled catchment. *Water Resources Research* **33**, 211–225.

Bachmair, S., and Weiler, M. (2012). Technical Report on Experimental Hillslope Hydrology, Hydronotes. University of Freiburg, Freiburg, Germany

Black J. R., Epstein E., Rains W. D., Yin Q. Z. and Casey W. H. (2008) Magnesium-isotope Fractionation During Plant Growth. *Environmental Science & Technology* **42**, 7831–7836.

Bolou-Bi E. B., Poszwa A., Leyval C. and Vigier N. (2010) Experimental determination of magnesium isotope fractionation during higher plant growth. *Geochimica et Cosmochimica Acta* **74**, 2523–2537.

621 Bolou-Bi E. B., Vigier N., Poszwa A., Boudot J.-P. and Dambrine E. (2012) Effects of
622 biogeochemical processes on magnesium isotope variations in a forested catchment in the
623 Vosges Mountains (France). *Geochimica et Cosmochimica Acta* **87**, 341–355.

624 Bouchez J., Blanckenburg F. von and Schuessler J. A. (2013) Modeling novel stable isotope
625 ratios in the weathering zone. *Am J Sci* **313**, 267–308.

626 Brenot A., Cloquet C., Vigier N., Carignan J. and France-Lanord C. (2008) Magnesium isotope
627 systematics of the lithologically varied Moselle river basin, France. *Geochimica et*
628 *Cosmochimica Acta* **72**, 5070–5089.

629 Brimhall G. H. and Dietrich W. E. (1987) Constitutive mass balance relations between chemical
630 composition, volume, density, porosity, and strain in metasomatic hydrochemical
631 systems: Results on weathering and pedogenesis. *Geochimica et Cosmochimica Acta* **51**,
632 567–587.

633 Campbell D. H., Clow D. W., Ingersoll G. P., Mast M. A., Spahr N. E. and Turk J. T. (1995)
634 Processes Controlling the Chemistry of Two Snowmelt-Dominated Streams in the Rocky
635 Mountains. *Water Resources Research* **31**, 2811–2821.

636 Cai, Di; Henehan, Michael; von Blanckenburg, Friedhelm; Uhlig, David (2021): Mg isotopic
637 composition of runoff is buffered by the regolith exchangeable pool. GFZ Data Services.
638 https://dataservices.gfz-
639 potsdam.de/panmetaworks/review/e91c6bb09610c102c8b650b0c81971f370c7d8c79851b
640 d61ff81d205720c553e/

641 Chapela Lara M., Buss H. L., Pogge von Strandmann P. A. E., Schuessler J. A. and Moore O. W.
642 (2017) The influence of critical zone processes on the Mg isotope budget in a tropical,
643 highly weathered andesitic catchment. *Geochimica et Cosmochimica Acta* **202**, 77–100.

644 Charlet L. and Sposito G. (1989) Bivalent ion adsorption by an oxisol. *Soil Science Society of*
645 *America Journal* **53**, 691–695.

646 Clow D. W. and Mast M. A. (2010) Mechanisms for chemostatic behavior in catchments:
647 Implications for CO2 consumption by mineral weathering. *Chemical Geology* **269**, 40–
648 51.

649 Dessert C., Lajeunesse E., Lloret E., Clergue C., Crispi O., Gorge C. and Quidelleur X. (2015)
650 Controls on chemical weathering on a mountainous volcanic tropical island: Guadeloupe
651 (French West Indies). *Geochimica et Cosmochimica Acta* **171**, 216–237.

652 Fahad Z. A., Bolou-Bi E. B., Kohler S. J., Finlay R. D. and Mahmood S. (2016) Fractionation and
653 assimilation of Mg isotopes by fungi is species dependent. Environ Microbiol Rep.

654 Feger, K.H., 1997. Biogeochemistry of magnesium in forest ecosystems. In Magnesium
655 deficiency in forest ecosystems. Springer, Dordrecht. pp. 67-99

656 Fries D. M., James R. H., Dessert C., Bouchez J., Beaumais A. and Pearce C. R. (2019) The
657 response of Li and Mg isotopes to rain events in a highly-weathered catchment. *Chemical*
658 *Geology* **519**, 68–82.

Galy A., Yoffe O., E. Janney P., W. Williams R., Cloquet C., Alard O., Halicz L., Wadhwa M., D. Hutcheon I., Ramon E. and Carignan J. (2003) Magnesium isotope heterogeneity of the isotopic standard SRM980 and new reference materials for magnesium-isotope-ratio measurements. Journal of Analytical Atomic Spectrometry 18, 1352–1356.

Ganor J., Roueff E., Erel Y. and Blum J. D. (2005) The dissolution kinetics of a granite and its minerals—Implications for comparison between laboratory and field dissolution rates. *Geochimica et Cosmochimica Acta* **69**, 607–621.

Godsey S. E., Kirchner J. W. and Clow D. W. (2009) Concentration–discharge relationships reflect chemostatic characteristics of US catchments. Hydrological Processes 23, 1844–1864.

Godsey S. E., Hartmann J. and Kirchner J. W. (2019) Catchment chemostasis revisited: Water quality responds differently to variations in weather and climate. Hydrological Processes 33, 3056–3069.

van der Heijden G., Legout A., Midwood A. J., Craig C.-A., Pollier B., Ranger J. and Dambrine E. (2013) Mg and Ca root uptake and vertical transfer in soils assessed by an in situ ecosystem-scale multi-isotopic (26Mg & 44Ca) tracing experiment in a beech stand (Breuil-Chenue, France). *Plant Soil* **369**, 33–45.

Hindshaw R. S., Teisserenc R., Le Dantec T. and Tananaev N. (2019) Seasonal change of geochemical sources and processes in the Yenisei River: A Sr, Mg and Li isotope study. *Geochimica et Cosmochimica Acta* **255**, 222–236.

Hindshaw R. S., Tosca R., Tosca N. J. and Tipper E. T. (2020) Experimental constraints on Mg isotope fractionation during clay formation: Implications for the global biogeochemical cycle of Mg. *Earth and Planetary Science Letters* **531**, 115980.

James J., Littke K., Bonassi T. and Harrison R. (2016) Exchangeable cations in deep forest soils: Separating climate and chemical controls on spatial and vertical distribution and cycling. *Geoderma* **279**, 109–121.

Jobbágy E. G. and Jackson R. B. (2001) The distribution of soil nutrients with depth: Global patterns and the imprint of plants. *Biogeochemistry* **53**, 51–77.

Jobbágy E. G. and Jackson R. B. (2004) The Uplift of Soil Nutrients by Plants: Biogeochemical Consequences Across Scales. *Ecology* **85**, 2380–2389.

Kim H., Bishop J. K. B., Dietrich W. E. and Fung I. Y. (2014) Process dominance shift in solute chemistry as revealed by long-term high-frequency water chemistry observations of groundwater flowing through weathered argillite underlying a steep forested hillslope. Geochimica et Cosmochimica Acta 140, 1–19.

Kim H., Dietrich W. E., Thurnhoffer B. M., Bishop J. K. B. and Fung I. Y. (2017) Controls on solute concentration-discharge relationships revealed by simultaneous hydrochemistry observations of hillslope runoff and stream flow: The importance of critical zone structure. *Water Resour. Res.* **53**, 1424–1443.

Kimmig S. R., Holmden C. and Bélanger N. (2018) Biogeochemical cycling of Mg and its

isotopes in a sugar maple forest in Québec. *Geochimica et Cosmochimica Acta*.

Lang F., Krüger J., Amelung W., Willbold S., Frossard E., Bünemann E. K., Bauhus J., Nitschke R., Kandeler E., Marhan S., Schulz S., Bergkemper F., Schloter M., Luster J., Guggisberg F., Kaiser K., Mikutta R., Guggenberger G., Polle A., Pena R., Prietzel J., Rodionov A., Talkner U., Meesenburg H., Wilpert K. von, Hölscher A., Dietrich H. P. and Chmara I. (2017) Soil phosphorus supply controls P nutrition strategies of beech forest ecosystems in Central Europe. *Biogeochemistry* **136**, 5–29.

Li W., Beard B. L., Li C. and Johnson C. M. (2014) Magnesium isotope fractionation between brucite [Mg(OH)2] and Mg aqueous species: Implications for silicate weathering and biogeochemical processes. *Earth and Planetary Science Letters* **394**, 82–93.

Liu X.-M., Teng F.-Z., Rudnick R. L., McDonough W. F. and Cummings M. L. (2014) Massive magnesium depletion and isotope fractionation in weathered basalts. Geochimica et Cosmochimica Acta 135, 336–349.

Ma L., Teng F.-Z., Jin L., Ke S., Yang W., Gu H.-O. and Brantley S. L. (2015) Magnesium isotope fractionation during shale weathering in the Shale Hills Critical Zone Observatory: Accumulation of light Mg isotopes in soils by clay mineral transformation. *Chemical Geology* **397**, 37–50.

Maher K., Johnson N. C., Jackson A., Lammers L. N., Torchinsky A. B., Weaver K. L., Bird D. K. and Brown G. E. (2016) A spatially resolved surface kinetic model for forsterite dissolution. *Geochimica et Cosmochimica Acta* **174**, 313–334.

Markewitz D., Davidson E. A., Figueiredo R. de O., Victoria R. L. and Krusche A. V. (2001) Control of cation concentrations in stream waters by surface soil processes in an Amazonian watershed. *Nature* **410**, 802–805.

Mavromatis V., Prokushkin A. S., Pokrovsky O. S., Viers J. and Korets M. A. (2014) Magnesium isotopes in permafrost-dominated Central Siberian larch forest watersheds. *Geochimica et Cosmochimica Acta* **147**, 76–89.

Miller E. K., Blum J. D. and Friedland A. J. (1993) Determination of soil exchangeable-cation loss and weathering rates using Sr isotopes. *Nature* **362**, 438–441.

Montgomery D. R. and Dietrich W. E. (2002) Runoff generation in a steep, soil-mantled landscape. Water Resources Research 38, 7-1-7–8.

Novak M., Farkas J., Kram P., Hruska J., Stepanova M., Veselovsky F., Curik J., Andronikov A. V., Sebek O., Simecek M., Fottova D., Bohdalkova L., Prechova E., Koubova M. and Vitkova H. (2020a) Controls on δ26Mg variability in three Central European headwater catchments characterized by contrasting bedrock chemistry and contrasting inputs of atmospheric pollutants. PLOS ONE 15, e0242915.

Novak M., Holmden C., Farkas J., Kram P., Hruska J., Curik J., Veselovsky F., Stepanova M., Kochergina Y. V., Erban V., Andronikov A., Sebek O., Koubova M., Bohdalkova L. and Vitkova H. (2020b) Magnesium and calcium isotope systematics in a headwater catchment underlain by amphibolite: Constraints on Mg–Ca biogeochemistry in an atmospherically polluted but well-buffered spruce ecosystem (Czech Republic, Central

738 Europe). CATENA 193, 104637.

739 Novak M., Andronikov A., Kram P., Curik J., Veselovsky F., Stepanova M., Prechova E., Sebek
740 O. and Bohdalkova L. (2021) Time-series of δ26Mg values in a headwater catchment
741 reveal decreasing magnesium isotope variability from precipitation to runoff.
742 *Hydrological Processes* **35**, e14116.

743 Oh N.-H. and Richter Jr. D. D. (2004) Soil acidification induced by elevated atmospheric CO2.
744 Global Change Biology 10, 1936–1946.

745 Opfergelt S., Burton K. W., Georg R. B., West A. J., Guicharnaud R. A., Sigfusson B., Siebert C.,
746 Gislason S. R. and Halliday A. N. (2014) Magnesium retention on the soil exchange
747 complex controlling Mg isotope variations in soils, soil solutions and vegetation in
748 volcanic soils, Iceland. *Geochimica et Cosmochimica Acta* **125**, 110–130.

749 Pogge von Strandmann P. A. E., Burton K. W., James R. H., van Calsteren P., Gislason S. R. and
750 Sigfússon B. (2008) The influence of weathering processes on riverine magnesium
751 isotopes in a basaltic terrain. *Earth and Planetary Science Letters* **276**, 187–197.

752 Pokharel R., Gerrits R., Schuessler J. A., Frings P. J., Sobotka R., Gorbushina A. A. and von
753 Blanckenburg F. (2018) Magnesium Stable Isotope Fractionation on a Cellular Level
754 Explored by Cyanobacteria and Black Fungi with Implications for Higher Plants.
755 *Environ. Sci. Technol.* **52**, 12216–12224.

756 Pokharel R., Gerrits R., Schuessler J. A. and von Blanckenburg F. (2019) Mechanisms of olivine
757 dissolution by rock-inhabiting fungi explored using magnesium stable isotopes. *Chemical*
758 *Geology* **525**, 18–27.

759 Poppe, L.J., Paskevich, V.F., Hathaway, J.C. and Blackwood, D.S., (2001). A laboratory manual
760 for X-ray powder diffraction. US Geological Survey open-file report, 1(041), 1-88.

761 Ryu J.-S., Jacobson A. D., Holmden C., Lundstrom C. and Zhang Z. (2011) The major ion,
762 δ44/40Ca, δ44/42Ca, and δ26/24Mg geochemistry of granite weathering at pH=1 and
763 T=25°C: power-law processes and the relative reactivity of minerals. *Geochimica et*
764 *Cosmochimica Acta* **75**, 6004–6026.

765 Ryu J.-S., Vigier N., Decarreau A., Lee S.-W., Lee K.-S., Song H. and Petit S. (2016)
766 Experimental investigation of Mg isotope fractionation during mineral dissolution and
767 clay formation. *Chemical Geology* **445**, 135–145.

768 Saenger C. and Wang Z. (2014) Magnesium isotope fractionation in biogenic and abiogenic
769 carbonates: implications for paleoenvironmental proxies. *Quaternary Science Reviews*
770 **90**, 1–21.

771 Salve R., Rempe D. M. and Dietrich W. E. (2012) Rain, rock moisture dynamics, and the rapid
772 response of perched groundwater in weathered, fractured argillite underlying a steep
773 hillslope. Water Resources Research 48.

774 Schmitt A.-D., Vigier N., Lemarchand D., Millot R., Stille P. and Chabaux F. (2012) Processes
775 controlling the stable isotope compositions of Li, B, Mg and Ca in plants, soils and
776 waters: A review. *Comptes Rendus Geoscience* **344**, 704–722.

Schott J., Mavromatis V., Fujii T., Pearce C. R. and Oelkers E. H. (2016) The control of carbonate mineral Mg isotope composition by aqueous speciation: Theoretical and experimental modeling. *Chemical Geology* **445**, 120–134.

Schuessler J. A., Kämpf H., Koch U. and Alawi M. (2016) Earthquake impact on iron isotope signatures recorded in mineral spring water. *Journal of Geophysical Research: Solid Earth* **121**, 8548–8568.

Shalev N., Farkaš J., Fietzke J., Novák M., Schuessler J. A., Strandmann P. A. E. P. von and Törber P. B. (2018) Mg Isotope Interlaboratory Comparison of Reference Materials from Earth-Surface Low-Temperature Environments. *Geostandards and Geoanalytical Research* **42**, 205–221.

Sohrt J., Uhlig D., Kaiser K., von Blanckenburg F., Siemens J., Seeger S., Frick D. A., Krüger J., Lang F. and Weiler M. (2019) Phosphorus Fluxes in a Temperate Forested Watershed: Canopy Leaching, Runoff Sources, and In-Stream Transformation. *Front. For. Glob. Change* **2**, 85.

Sprenger M., Seeger S., Blume T. and Weiler M. (2016) Travel times in the vadose zone: Variability in space and time. Water Resources Research 52, 5727–5754.

Teng F.-Z. (2017) Magnesium Isotope Geochemistry. *Reviews in Mineralogy and Geochemistry* **82**, 219–287.

Teng F.-Z., Li W.-Y., Rudnick R. L. and Gardner L. R. (2010) Contrasting lithium and magnesium isotope fractionation during continental weathering. Earth and Planetary Science Letters 300, 63–71.

Tipper E. T., Galy A. and Bickle M. J. (2008) Calcium and magnesium isotope systematics in rivers draining the Himalaya-Tibetan-Plateau region: Lithological or fractionation control? *Geochimica et Cosmochimica Acta* **72**, 1057–1075.

Tipper E. T., Galy A. and Bickle M. J. (2006a) Riverine evidence for a fractionated reservoir of Ca and Mg on the continents: Implications for the oceanic Ca cycle. *Earth and Planetary Science Letters* **247**, 267–279.

Tipper E. T., Galy A., Gaillardet J., Bickle M. J., Elderfield H. and Carder E. A. (2006b) The magnesium isotope budget of the modern ocean: Constraints from riverine magnesium isotope ratios. *Earth and Planetary Science Letters* **250**, 241–253.

Tipper E. T., Lemarchand E., Hindshaw R. S., Reynolds B. C. and Bourdon B. (2012) Seasonal sensitivity of weathering processes: Hints from magnesium isotopes in a glacial stream. *Chemical Geology* **312–313**, 80–92.

Trivedi P. and Axe L. (2001) Predicting Divalent Metal Sorption to Hydrous Al, Fe, and Mn Oxides. *Environ. Sci. Technol.* **35**, 1779–1784.

Uhlig D., Amelung W. and Blanckenburg F. von (2020) Mineral Nutrients Sourced in Deep Regolith Sustain Long-Term Nutrition of Mountainous Temperate Forest Ecosystems. *Global Biogeochemical Cycles* **34**, e2019GB006513.

Uhlig D. and von Blanckenburg F. (2019) How Slow Rock Weathering Balances Nutrient Loss During Fast Forest Floor Turnover in Montane, Temperate Forest Ecosystems. *Front. Earth Sci.* **7**.

Uhlig D., Schuessler J. A., Bouchez J., Dixon J. L. and von Blanckenburg F. (2017) Quantifying nutrient uptake as driver of rock weathering in forest ecosystems by magnesium stable isotopes. *Biogeosciences* **14**, 3111–3128.

Wimpenny J., Burton K. W., James R. H., Gannoun A., Mokadem F. and Gíslason S. R. (2011) The behaviour of magnesium and its isotopes during glacial weathering in an ancient shield terrain in West Greenland. *Earth and Planetary Science Letters* **304**, 260–269.

Wimpenny J., Colla C. A., Yin Q.-Z., Rustad J. R. and Casey W. H. (2014) Investigating the behaviour of Mg isotopes during the formation of clay minerals. *Geochimica et Cosmochimica Acta* **128**, 178–194.

Wimpenny J., Gíslason S. R., James R. H., Gannoun A., Pogge Von Strandmann P. A. E. and Burton K. W. (2010) The behaviour of Li and Mg isotopes during primary phase dissolution and secondary mineral formation in basalt. *Geochimica et Cosmochimica Acta* **74**, 5259–5279.

Brady N. C. and Weil R. R. (2008) The Nature and Properties of Soils., Prentice Hall.

Yu Z., Chen H. Y. H., Searle E. B., Sardans J., Ciais P., Peñuelas J. and Huang Z. (2020) Whole soil acidification and base cation reduction across subtropical China. *Geoderma* **361**, 114107.